In-situ visualization of the enzymatic growth of surface-immobilized DNA block copolymer micelles by scanning force microscopy

Wang, Jie; Alemdaroglu, Fikri E.; Prusty, Deepak K.; Herrmann, Andreas; Berger, Ruediger

Published in:
Macromolecules

DOI:
10.1021/ma701937u

Publication date:
2008

In-Situ Visualization of the Enzymatic Growth of Surface-Immobilized DNA Block Copolymer Micelles by Scanning Force Microscopy

Jie Wang, Fikri E. Alemdaroglu, Deepak K. Prusty,† Andreas Herrmann,*,† and Rüdiger Berger*

Max Planck Institute for Polymer Research, Ackermannweg 10, 55128, Mainz, Germany

Received August 28, 2007; Revised Manuscript Received February 1, 2008

ABSTRACT: The enzymatic growth of diblock copolymer micelles consisting of single-stranded DNA and poly(propylene oxide) (PPO) segments was studied with scanning force microscopy (SFM). DNA-*b*-PPO aggregates adsorbed randomly on a mica surface exhibiting a height of 4–5 nm. The size of the micelles was increased by terminal deoxynucleotidyl transferase (TdT), which catalyzes the repetitive addition of deoxyribonucleotides to the 3′-hydroxyl end of DNA. The onset of the micelle growth was controlled by the addition of 2′-deoxythymidine 5′-triphosphate (dTTP) mononucleotide to the reaction solution or by increasing the temperature to 37 °C. We determined the mean heights of the micelles from statistical analysis of SFM pictures recorded at different reaction times in-situ. The arrangements, heights, and lateral sizes of individual micelles were also followed. After 60 min a plateau in micelle height was observed (6–8 nm). In contrast, micelles that were grown in solution, i.e., in the absence of a mica surface, showed no saturation effect for the same reaction time. The interaction of DNA with the surface and the hindered exchange of the block copolymers are proposed as possible reasons for the saturation in the growth of micelles adsorbed on mica. From a simple geometrical model, we estimated the number of extended mononucleotides.

Introduction

Scanning force microscopy (SFM) allows the direct visualization of DNA molecules, their conformation, interaction, and assembly in near-physiological environments[1,2] and the investigation of single-molecular mechanics.[3] The SFM has for example been used by Guthold et al. to observe nonspecific and specific binding of RNA polymerase to DNA molecules adsorbed on mica under aqueous conditions,[4,5] and van Noort et al. were able to use the SFM to visualize dynamic photolyase−DNA interactions, including association, dissociation, and movement of photolyase over the DNA.[6] Single enzyme molecules and enzymatic activities have been observed,[7–9] and in recent years researchers have started investigating pathways of activation of enzymes and proposed models for enzymatic processes based on SFM techniques.[10,11]

Terminal deoxynucleotidyl transferase (TdT) is an enzyme which belongs to the family of polymerases called pol X and is responsible for the generation of the random genetic information that is essential for the efficacious function of the vertebrate adaptive immune system.[12] TdT catalyzes the repetitive addition of deoxyribonucleotides to the 3′ hydroxyl ends of DNA in a template-independent manner[13] and has been used to extend DNA in solution.[14] For example, TdT can be used for homopolymeric tailing in molecular cloning[15] or to label DNA at the 3′ ends for chemical nucleotide sequencing.[16] In 2005, Chow et al. studied the ability of TdT to catalyze the surface-initiated polymerization of DNA.[17] Thereby, the height of self-assembled oligonucleotide monolayers on regular gold patterns was extended vertically. The height increase was confirmed by SFM and recorded in air after the reaction. The dimensions of the square surface pattern were gradually varied from 100 nm to 4 μm. It turned out that the vertical extension with DNA was dependent on the lateral feature size of the underlying gold patterns. The decrease in the vertical extension for smaller feature sizes was attributed to an increase in the conformational mobility of the DNA chains. It was assumed that this reduced the accessibility of TdT or mononucleotides to the 3′ ends of the growing single-stranded polynucleotides.

A patterning method not relying on lithography is based on the phase separation of block copolymers, allowing one to fabricate small features down to a few nanometers in diameter.[18] In dilute aqueous solutions, linear amphiphilic polyelectrolyte block copolymers self-assemble into three-dimensional spherical micelles with a charged corona and a hydrophobic core.[19] Such nanocontainers were applied as drug delivery vehicles, where lipophilic drugs were incorporated into their hydrophobic interior.[20] Recently, a novel type of bioorganic block copolymer was introduced, which consisted of a hydrophobic segment, e.g., poly(propylene oxide) (PPO), that was covalently linked to DNA.[21] The resulting micelles could be used as three-dimensional scaffolds for DNA-templated organic reactions.[22] Moreover, the size of these nanoparticles could be adjusted by employing the DNA block copolymer aggregates as priming species for the TdT enzyme.[23] In regard to the morphology, hybridization of single-stranded DNA micelles with long nucleic acid template molecules resulted in structure changes from a sphere to rodlike shape.[24] Furthermore, the scaling behavior of polymeric and biopolymeric nanostructures fabricated by surface-initiated polymerization has recently been studied by Lee et al.[25] Here, patterns ranging in lateral size from 100 nm to 4 μm were studied.

Here we report an in-situ analysis of the growth of DNA-*b*-PPO diblock copolymer micelles immobilized on a surface mediated by the TdT enzyme based on SFM measurements (Scheme 1). In contrast to lithographically defined patterns, DNA-*b*-PPO aggregated with a diameter of tens of nanometers, adsorbed randomly on a mica surface, and allowed the observation of individual structures. The enzymatic growth of DNA-*b*-PPO micelles extended the range of patterns sizes down to the scale of tens of nanometers. The onset of growth was controlled by temperature or by the addition of 2′-deoxythy-

* To whom correspondence should be addressed. E-mail: a.herrmann@rug.nl; berger@mpip-mainz.mpg.de.

† Current address: University of Groningen, Zernike Institute for Advanced Materials, Nijenborgh 4, 9747 AG Groningen, The Netherlands.

10.1021/ma701937u CCC: $40.75
Published on Web 03/27/2008

Scheme 1. Diagram Showing the Growth of the DNA-*b*-PPO Diblock Copolymer Micelles on Mica in a Buffer Solution in the Presence of TdT, Co^{2+}, and dTTP

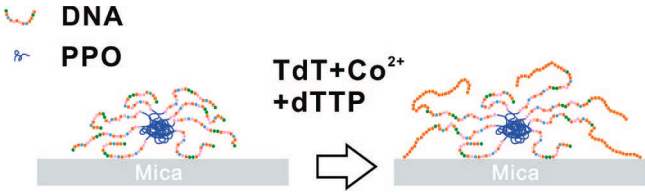

midine 5′-triphosphate (dTTP) mononucleotide to the reaction solution.

Experimental Section

Materials. *DNA-b-poly(propylene oxide) (PPO).* The DNA-*b*-PPO contained a nucleic acid unit consisting of 22 nucleotides (sequence: 5′-CCTCGCTCTGCTAATCCTGTTA-3′, M_w: 6612 g/mol) or 42 nucleotides (sequence: 5′-CCTCGCTCTGCTAATC-CTGTTATTTTTTTTTTTTTTTTTTT-3′, M_w: 12 696 g/mol) and a synthetic polymer block of $M_w = 6800$ g/mol. The synthesis has been reported elsewhere.[22]

Enzyme and Chemicals. Terminal deoxynucleotidyl transferase (TdT, 20 U/μL), 2′-deoxythymidine 5′-triphosphate (dTTP, 10 mM) and the 5× reaction buffer (1 M potassium cacodylate, 0.125 M Tris, 0.05% (v/v) Triton X-100, 5 mM $CoCl_2$, pH 7.2 at 25 °C) were purchased from Fermentas (St. Leon-Rot, Germany). The SFM imaging buffer (10 mM Tris pH 7.4, 1 mM $NiCl_2$) was prepared with MilliQ water.

Mica. Mica sheets (Plano GmbH, Germany) were glued to steel disks with epoxy resin and cleaved with tape immediately before use.

Scanning Force Microscopy (SFM). In order to observe the growth of micelles in-situ by SFM, an experimental procedure had to be developed that did not inhibit the activity of TdT and which allowed the stable imaging of PPO-*b*-DNA micelles. We found that the following procedure fulfilled the above requirements: A drop of 20 μL of the reaction mixture was deposited onto freshly cleaved mica. The droplet contained 1 μL of 1.8 mg/L DNA-*b*-PPO, 2 μL of 20 U/μL TdT, 4 μL of the 5× enzyme reaction buffer, and 13 μL of the imaging buffer. The final concentration of DNA-*b*-PPO and TdT was 90 μg/L and 2 U/μL, respectively.

After an incubation time of 10 min on the mica surface, the sample was diluted with 150 μL of imaging buffer, by carefully pouring the buffer solution over the mica onto a piece of filter paper without allowing the mica surface to dry. The mica was then covered with 50 μL of the imaging buffer. Afterward, the mica sheet was mounted in the SFM. The measurements were carried out in an O-ring sealed glass liquid cell, which was filled with buffer solution. The temperature in the liquid cell could be controlled with an accuracy of ±0.1 °C. When a temperature of 37 °C was reached, 2 μL of 10 mM dTTP was injected into the liquid cell.

The images were recorded in liquid using a scanning force microscope (MultiMode, Nanoscope IIIa, Veeco Instruments, Santa Barbara, CA), which was operated in the soft tapping mode. A piezoelectric J-scanner (Veeco Instruments) was used, which was equipped with a thermal application controller (Veeco Instruments).

Oxide-sharpened silicon nitride cantilevers (NP-S, Veeco Instruments; 115 μm long, 17 μm wide, 0.6 μm thick) with an integrated tip (nominal tip radius 10 nm; spring constant 0.32 N/m, and resonance frequency of 56 kHz in air) were used. The tips were cleaned with argon plasma and ethanol before measurements. The height of the tip was 2.5−3.5 μm. The tip radius was confirmed by scanning electron microscopy, after having performed the SFM measurements.

We selected a driving frequency between 8 and 10 kHz for imaging in liquid. SFM images (512 × 512 pixels) were recorded at a scan rate of 1 Hz. Images were processed by a first-order flattening, in order to remove the background slope. The maximum height of individual globular structures was determined by means of local roughness analysis. All height data were then plotted together in the histograms. The results are expressed as the mean ± full width at half-maximum height of the Gaussian fits (fwhm).

Results and Discussion

Enzymatic reactions were controlled by adding dTTP mononucleotides to the buffer solution containing TdT enzymes or by the temperature of the reaction solution.

Control by Adding dTTP Mononucleotides. After the sample was mounted to the SFM microscope, the fluid cell was immediately filled with imaging buffer. Then the sample was heated from 22 to 37 °C at a rate of 1.6 °C/min. After reaching a temperature of 37 °C the sample surface was investigated (Figure 1A). Globular structures were observed, showing a small variation in height and size. We found that the structures did not change with time and therefore constituted a defined starting point. We injected 2 μL of 10 mM dTTP mononucleotide into the fluid cell, which defined $T = 0$ min for the enzymatic reaction. Afterward, successive SFM images were captured, while all parameters were kept constant (Figure 1B−E). The topography at 20 and 40 min showed that part of the structures on the surface started to grow vertically and laterally. Subsequent SFM images indicated that this growth continued until ∼60 min. SFM topography images recorded at 134 and 540 min showed no significant changes compared to those measured at 60 min. In order to analyze the growth process in more detail, we collected the height data of ∼300 surface features for images recorded at $T = 0$, 20, 40, 134, and 540 min and plotted them in histograms (Figure 1F). Each histogram is composed of two peaks, which were fitted by Gaussian distributions. In the case of the structures observed at $T = 0$ min, the Gaussian distribution revealed a peak at 3.0 ± 0.5 nm and another peak at 4.5 ± 1.3 nm. The position and the shape of the first peak around 3 nm remained uniform after the injection of dTTP ($T = 20$ min: 2.7 ± 0.4 nm; $T = 40$ min: 2.8 ± 0.5 nm; $T = 134$ min: 2.9 ± 0.4 nm; and $T = 540$ min: 2.7 ± 0.5 nm). Therefore, we assigned this peak to TdT enzymes on the surface. The second peak shifted from 4.5 ± 1.3 nm at $T = 0$ min, to 5.0 ± 2.3 nm at $T = 20$ min, to 5.7 ± 2.7 nm at $T = 40$ min, and to 6.3 ± 2.9 nm at $T = 134$ min. As this increase indicates the growth of structures, the second peak was assigned to DNA-*b*-PPO micelles participating in the enzymatic reaction. The histograms obtained after 134 min reaction time did not show a further shift in the peak position, i.e., the mean height of the DNA-*b*-PPO micelles.

As both TdT and DNA-*b*- PPO micelles have similar sizes at the beginning, we performed two control experiments with either only TdT or DNA-*b*-PPO micelles in buffer solution (Figure 2A,B). This separate analysis of TdT and DNA-*b*-PPO micelles allowed us to obtain a more precise size distribution of both constituents. The histogram of the analyzed heights of the TdT enzymes revealed a maximum at 3.2 ± 1.2 nm (Figure 2C). In contrast to the TdT enzyme, we determined an average height of the DNA-*b*-PPO micelles of 4.3 ± 2.0 nm (Figure 2D). These results agree with our above assignments of the peaks.

The integral value of the Gaussian fits for TdT enzymes and DNA-*b*-PPO micelles were found to be independent of the time of enzymatic reaction. This indicates that the number of structures observed remained constant and that they did not desorb from the surface or were not moved by the scanning process to the edge of the scan area. Furthermore, the development of the two peaks, as seen from our statistical analysis, showed that most micelles participated in the enzymatic reactions. The mean height data that were determined by the Gaussian peak of the fitted histograms of the DNA-*b*-PPO micelles are plotted in Figure 3 (filled circles). The height of

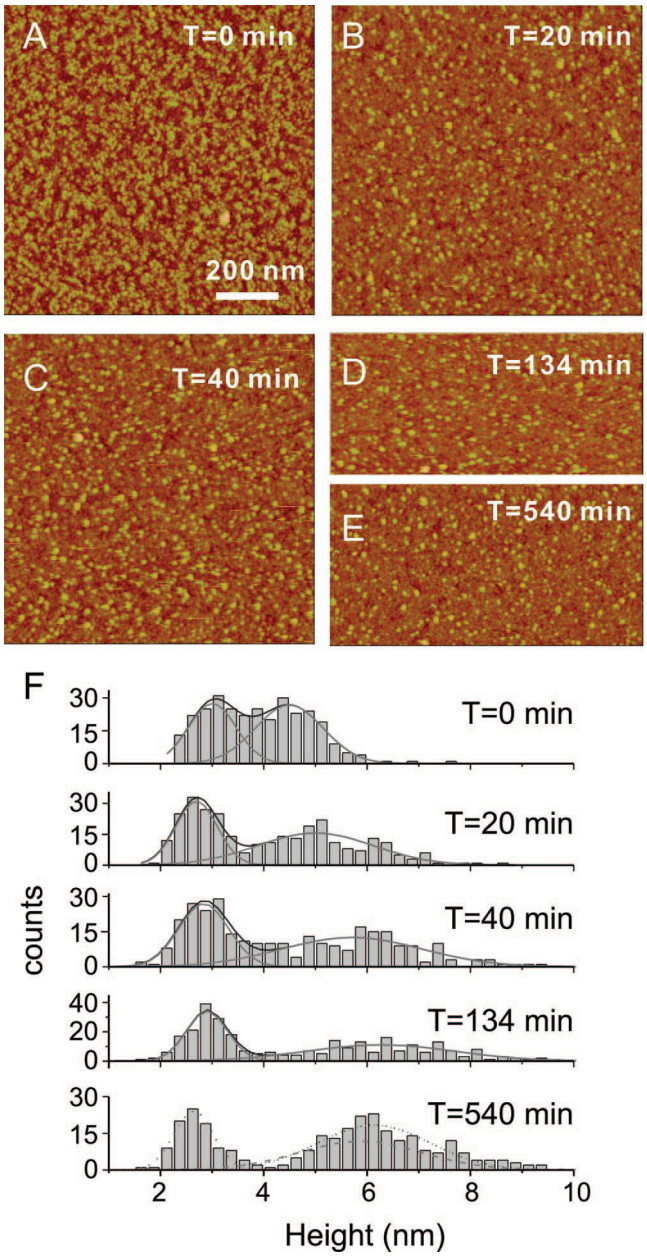

Figure 1. Selected time-lapse SFM images of the reaction mixture before and after the injection of dTTP to the liquid cell at 37 °C and the height distribution of the surface structures. (A) Before injection of dTTP, (B) 20 min after the injection of dTTP, (C) 40 min after the injection of dTTP, (D) 134 min after the injection of dTTP, and (E) 540 min after the injection of dTTP. The lateral scale is 200 nm, and the height scale is 15 nm for all images. (F) Histograms of height of globular structures obtained from SFM measurements. Each histogram was fitted by two Gaussian distributions. At a reaction time $T = 540$ min, we changed the surface area, which was imaged and found to have a mean height of micelles of 6.1 ± 1.1 nm (dotted line). This value is close to the height of micelles obtained at the original position. In addition, a new tip was used for imaging after 1440 min and revealed a mean height of micelles of 5.9 ± 1.2 nm (dashed line) not significantly different from the height of micelles at 540 min.

the micelles reached a plateau after about 1 h. This result is consistent with the observation from previous measurements on surface-initiated polymerization of grafted DNA chains.[17]

Interestingly, some micelles seem to grow faster than others, a result seen from the change in the width of the Gaussian distribution (open circles in Figure 3). We define fwhm as the full width of the histogram at half-maximum height. The fwhm increased in the beginning of the reaction from 1.6 ± 0.2 to

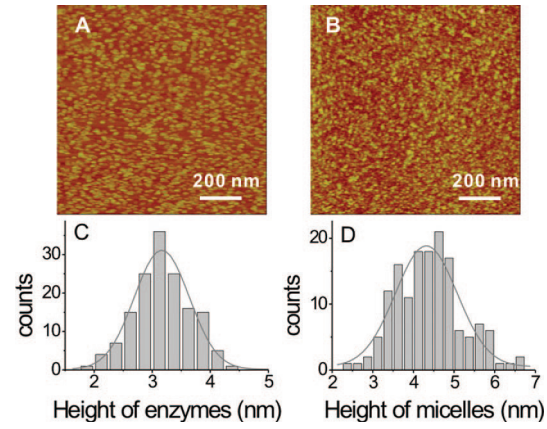

Figure 2. Pure TdT and DNA-*b*-PPO diblockcoplymer micelles imaged by tapping mode SFM in buffer and their distributions of height. (A) TdT at a concentration of 0.2 U/μL in the imaging buffer solution. (B) DNA-*b*-PPO at a concentration of 180 μg/L in the imaging buffer solution. In both cases, the substrate was freshly cleaved mica and the height scale is 15 nm. (C) Histogram of the height of TdT obtained from (A). (D) Histogram of the height of the DNA-*b*-PPO micelles obtained from (B). Both histograms were fitted by a Gaussian distribution.

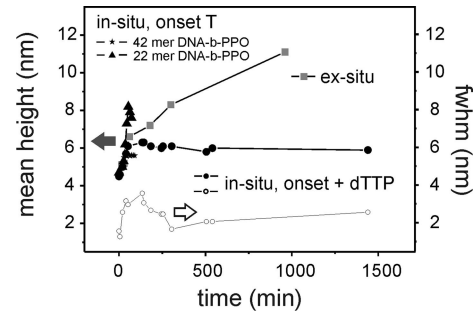

Figure 3. Variations of the mean height of DNA-*b*-PPO micelles and the full width of the histogram at half-maximum height (fwhm) as a function of the reaction time for the in-situ and ex-situ measurements: "onset T" stands for a control of enzymatic reaction by temperature (37 °C), and "onset + dTTP" stands for starting of the enzymatic reaction by adding monomers. Filled symbols correspond to mean height axis shown on the left, and open symbols correspond to full width half-maxima (fwhm) given on the right side.

3.6 ± 0.4 nm 134 min after the injection of the dTTP mononucleotide. This value was then found to decrease to 2.1 ± 0.3 nm at a time of 505 min after the injection. The reduction in the width of the Gaussian distribution indicates that the enzymatic reaction was slowed down or was disabled after a certain length of DNA was reached, while at the same time, shorter DNA strands could be still extended by TdT. In order to confirm that the size distribution of micelles was representative, two reference experiments were performed at $T = 540$ min and $T = 1440$ min. First, we varied the surface area, which was investigated by SFM (dotted line Figure 1F). Second, we changed the SFM tip in order to exclude artifacts from the tip shape (dashed line of Figure 1F). Both reference experiments did not show any significant variation on the reported data. Furthermore, tip artifacts could be excluded, since enzymes with lower heights were still resolvable while micelles with larger sizes were being imaged (Figure 1A−E).

We next would like to consider the reason for the termination of the TdT catalysis of micelle nanostructures on the surface. In order to exclude a reduction of monomer access or a change in TdT catalytic behavior over time, we performed a control experiment with a DNA-*b*-PPO polymer exhibiting a significantly longer DNA segment composed of 42 bases. We found

that the saturation in growth was reached 28 min after the initiation of the reaction, which was about 30 min earlier than that in the experiment with the 22 mer DNA-*b*-PPO micelles. Thus, a reduction of monomer access and changes in catalytic behavior played a minor role. It also suggests that DNA-*b*-PPO interacted with the mica surface in a way that significant further growth could not be observed after the DNA segment had reached a certain length.

To elucidate the size of DNA-*b*-PPO micelle nanostructures independent of the influence of a surface, we performed the enzymatic reactions ex-situ.[23] This was done by incubating the micelles in a buffer solution with TdT and dTTP at 37 °C in a thermoshaker. Samples were taken at certain time intervals (15, 30, 60, 300, and 960 min) and investigated by SFM in the buffer solution at room temperature (23 °C). Compared to the in-situ growth, the ex-situ growth showed no saturation effect (Figure 3, gray filled squares). In particular, the growth in both experiments showed the same slope of 0.03 nm/min for reaction times <60 min. Thus, we conclude that the surface must play the major role in saturation of growth. In the ex-situ reaction, growth in the size of the micelles in solution might be mediated by exchange of DNA-*b*-PPO molecules of micelles with single molecules in solution.[26,27] As reported, the residence time of the block copolymer molecules in the micelles could be on the order of 1 h,[28] which fits to the time scale of our experiments. The exchange of molecules can also be noticed by the size distribution of micelles recorded after 60 min of ex-situ reaction compared to the one recorded in the in-situ reaction. For the ex-situ reaction, we determined a fwhm, which was 2.2 ± 0.2 nm (histogram provided in the Supporting Information). This width was significantly smaller than that one of the in-situ experiment of the micelles for a time of 52 min (fwhm = 3.0 ± 0.3 nm). In solution, all DNA-*b*-PPO molecules have the same probability to react with dTTP in the presence of TdT and exchange of DNA-*b*-PPO molecules in micelles and in solution takes place which lead to a more even distribution of the length of DNA-*b*-PPO molecules in micelles. Both are not the case for DNA-*b*-PPO molecules of immobilized micelles on the mica surface. In particular, exchange of DNA-*b*-PPO molecules of micelles with single molecule in solution was significantly reduced for micelles adsorbed onto mica.

One effect leading to the termination of the TdT catalysis of immobilized micelles composed of DNA-*b*-PPO molecules could be that, after reaching a certain length, the DNA segments fold back into the DNA corona and block the catalytic site. The persistence length of a single-stranded DNA is 0.75−1.3 nm.[29–31] It is shorter than the length of the DNA segment in micelles before enzymatic reaction (3.3 nm). However, in micelles the DNA-*b*-PPO molecules are ordered that could result in an increase in length upon which significant back folding can occur. In addition, we must consider that as the DNA segment becomes longer, the surface interaction could also result in prevention of catalysis. In the case that the latter effect was the dominant contribution, the enzymatic growth would be terminated only at the edges of patterns composed of self-assembled oligonucleotide monolayers on gold.[17]

Continuous Monitoring of Selected Micelles. The catalytic reaction can also be initiated solely by controlling the reaction temperature to the temperature optimum of TdT. In this way, we can avoid the drift of the surface relative to the SFM tip, which may be induced by the injection of dTTP. We therefore prepared 20 μL of the reaction mixture, which contained all the components for the enzymatic reaction, and controlled the onset of the reaction by increasing the temperature to 37 °C. The reaction mixture contained 1 μL of 1.8 mg/L PPO-*b*-DNA, 2 μL of 20 U/μL TdT, 2 μL of 10 mM dTTP, 4 μL of 5 × enzyme reaction buffer, and 11 μL of imaging buffer. The final

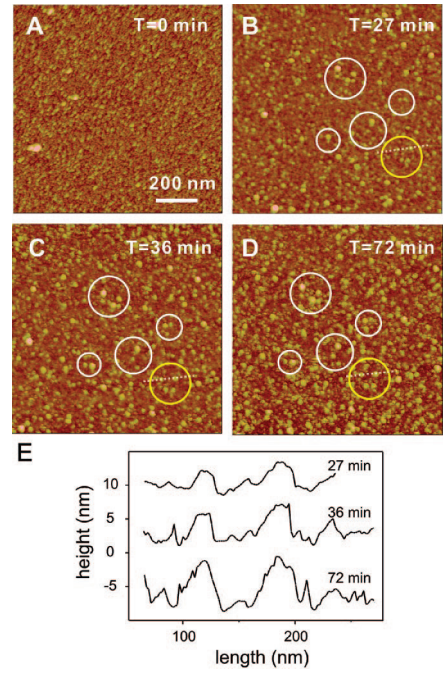

Figure 4. Selected time-lapse SFM images of the reaction mixture before and after the temperature was increased to 37 °C. Lateral scale bar: 200 nm. The height scale is 15 nm. (A) Before heating. (B) 27 min after 37 °C was reached. (C) 36 min after 37 °C was reached. (D) 72 min after 37 °C was reached. (E) Height profiles along the line in Figure 3B−D.

respective concentration of PPO-*b*-DNA, TdT, and dTTP were 90 μg/L, 2 U/μL, and 1 mM in a Ni^{2+} containing 1× reaction buffer.

Figure 4A shows the image recorded at room temperature (23 °C) and corresponds to the reaction time $T = 0$ min. The temperature of the mixture was increased to 37 °C at a rate of 1.6 °C/min, in order to start the reaction. The surface was imaged again 18 min after reaching 37 °C (Figure 4B). The SFM image shows that the height of some globular structures increased. We continued to image the surface at 37 °C and kept all scanning parameters constant (Figure 4C,D). In this way, we were able to follow the size and arrangement of individual structures on the surface; e.g., the features marked by the circles could be recognized and compared in different images. We made topographical profiles (Figure 4E) of the two structures inside the yellow circle at $T = 27$, 36, and 72 min along the dotted line which is indicated in the figures. The left structure increased its height by 86% from 3.5 to 6.5 nm and the right one by 89% from 3.6 to 6.8 nm. From this we concluded that these structures were DNA-*b*-PPO micelles, which grew both vertically and laterally in the presence of TdT.

In order to obtain a better statistic of the structures undergoing changes, we collected the height data of 300 surface features at $T = 0$, 27, 36, and 72 min and plotted them in histograms (histograms are provided in the Supporting Information). The increase in the mean height of the micelles, determined from the Gaussian fits, can be seen from Figure 3 (filled triangles). In the temperature-controlled experiment, the mean height of the micelles stopped increasing after about 1 h. This time is similar to the time observed for the TdT reaction initiated by the mononucleotide addition.

Calculation of the Number of T-Bases Added to DNA-*b*-PPO. The average height and radius of the DNA-*b*-PPO micelles could be correlated to the average number of mononucleotides added to DNA-*b*-PPO molecules. Here, we assume that the DNA

Scheme 2. Diagram Showing the Model of Imaging a DNA-*b*-PPO Micelle with an SFM Tip[a]

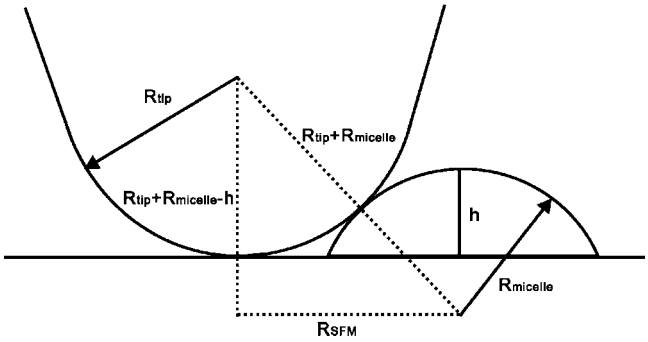

[a] R_{tip} is the tip radius of curvature, $R_{micelle}$ is the radius of the micelle, h is the measured height of the micelle, and R_{SFM} is the measured radius of the micelle.

segments are freely jointed chains and that the length of a DNA-*b*-PPO molecule is

$$L = \sqrt{N_{base}} l_{base} + R_{PPO} \quad (1)$$

where N_{base} is the number of bases, l_{base} is the length per base, and R_{PPO} is the gyration radius of PPO.[32] Before the enzymatic reaction, N_{base} was 22. Also, we assumed 0.7 nm/base for single-stranded DNA considering results determined using different approaches[29,33,34] in order to calculate l_{base}. Finally, R_{PPO} for a molecular weight of 6800 g/mol was 2.0 nm.[35] We can obtain the length of the DNA segment in micelles from eq 1 as 3.3 nm and the length of the DNA-*b*-PPO molecule as $L = 5.3$ nm before the enzymatic process at $T = 0$ min.

Next, we used simple geometrical models in order to estimate the number of bases added (Scheme 2). The tip can be modeled as a cone with a spherical end (radius of curvature R_{tip}). In our experiment, the radius of the micelle is similar to the radius of the tip. We can therefore determine $R_{micelle}$ using the Pythagoream theorem.

$$(R_{tip} + R_{micelle} - h)^2 + {R_{SFM}}^2 = (R_{tip} + R_{micelle})^2 \quad (2)$$

In this equation, R_{tip} is the tip radius of curvature, $R_{micelle}$ is the radius of the micelle, h is the measured height of the micelle, and R_{SFM} is the measured radius of the micelle. R_{SFM} and h can be obtained using the statistical analysis of the SFM images. In the initial case, before the enzymatic reaction, $R_{SFM} = 10.2$ nm and $h = 4.7$ nm (Figure 4A). The tip radius of curvature R_{tip} was 8 nm. The radius of the micelle $R_{micelle}$ could therefore be calculated to be $R_{micelle} = 5.4$ nm. If we assume that the length of the DNA-*b*-PPO molecule is equal to $R_{micelle}$, then according to eq 1 the number of bases in the DNA-*b*-PPO molecule must be 24, which is a value that is 9.1% different than the actual number of bases (22) before the enzymatic reaction. We also imaged 42-mer DNA-*b*-PPO micelles using scanning force microscopy and measured the radius and height of the micelles. The values were 14.0 and 4.5 nm, respectively. The tip radius of curvature was 17 nm. In this case, the number of bases was calculated using eqs 1 and 2 to be 52. Here there was a difference of 23.8% compared with the actual number of bases (42). A topographic image of these micelles and the SEM image of the tip can be found in the Supporting Information.

After an enzymatic reaction time of 72 min, we obtained a radius of micelle R_{SFM} of 13.4 nm and a mean height h of 7.6 nm from the SFM measurement. According to eq 2, we could obtain the radius of the micelle $R_{micelle}$ to be 7.6 nm. If we assume that the length of the DNA-*b*-PPO molecule is equal to $R_{micelle}$ ($L = R_{micelle} = 7.6$ nm), then we can calculate the number of bases N_{base} from eq 1 to be 64. The number of added bases

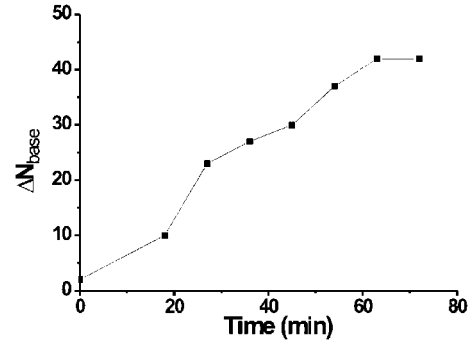

Figure 5. Plot of the number of extended T-bases vs reaction time for the in-situ experiment when the reaction was controlled by temperature.

to DNA-*b*-PPO within a micelle is in average $\Delta N_{base} = 64 - 22 = 42$, after 72 min of enzymatic reaction. On the basis of the above-discussed estimation, we calculated the extension of DNA-*b*-PPO molecules within micelles for all SFM images obtained from the reaction initiated by temperature (Figure 5).

Summary and Conclusion

We used the SFM to investigate the catalytic reaction of TdT enzymes with DNA-*b*-PPO micelles as the priming species on mica surface in situ. This is the first time that the size of the micelles has been very precisely adjusted by an enzyme on a mica surface. Additionally, it demonstrated that the growth of micelles could be initiated by adding 2′-deoxythymidine 5′-triphosphate (dTTP) mononucleotides to the reaction solution or by adjusting the reaction temperature to 37 °C. The growth of individual micelles could be followed. Statistical analysis showed that in both cases the height of micelles saturated after about 1 h. In contrast, micelles that were grown in solution, i.e., in the absence of a mica surface, showed no saturation effect within the same reaction time. The comparison between ex-situ and in-situ growth behavior of the same micelle system allows us to attribute the saturation effect to the DNA−surface interaction and the reduced exchange of DNA-*b*-PPO molecules within the micelles and in the buffer solution. We constructed a geometrical model that considered the tip radius of curvature in order to extract the number of nucleotides that were added by the catalytic reaction.

Acknowledgment. This work was supported by DFG-Sonderforschungsbereich 625 “From Single Molecules to Nanoscopically Structured Materials”. We acknowledge Hans Jürgen Butt and Klaus Müllen for continuous fruitful discussions and support. We are grateful to Uwe Rietzler for supporting the SFM measurements, to Kaloian Koynov and Thipphaya Cherdhirankorn for FCS measurements, and to Maren Müller for characterization of cantilever tips with SEM.

Supporting Information Available: SEM imaging of a cantilever tip after the in-situ measurement, comparison of the histograms for in-situ and ex-situ experiments, AFM imaging and enzymatic reaction of 42-mer DNA-*b*-PPO, height distribution of surface structures in the experiment “continuous monitoring of selected micelles”, and gel electrophoresis pictures of the DNA-*b*-PPO block copolymers after different reaction times in the presence and in the absence of Ni^{2+}. This material is available free of charge via the Internet at http://pubs.acs.org.

References and Notes

(1) Hansma, H. G. *Annu. Rev. Phys. Chem.* **2001**, *52*, 71–92.
(2) Rothemund, P. W. K. *Nature (London)* **2006**, *440*, 297–302.

(3) Severin, N.; Zhuang, W.; Ecker, C.; Kalachev, A. A.; Sokolov, I. M.; Rabe, J. P. *Nano Lett.* **2006**, *6*, 2561–2566.
(4) Guthold, M.; Bezanilla, M.; Erie, D. A.; Jenkins, B.; Hansma, H. G.; Bustamante, C. *Proc. Natl. Acad. Sci. U.S.A.* **1994**, *91*, 12927–12931.
(5) Guthold, M.; Zhu, X. S.; Rivetti, C.; Yang, G. L.; Thomson, N. H.; Kasas, S.; Hansma, H. G.; Smith, B.; Hansma, P. K.; Bustamante, C. *Biophys. J.* **1999**, *77*, 2284–2294.
(6) van Noort, S. J. T.; van der Werf, K. O.; Eker, A. P. M.; Wyman, C.; de Grooth, B. G.; van Hulst, N. F.; Greve, J. *Biophys. J.* **1998**, *74*, 2840–2849.
(7) Bezanilla, M.; Drake, B.; Nudler, E.; Kashlev, M.; Hansma, P. K.; Hansma, H. G. *Biophys. J.* **1994**, *67*, 2454–2459.
(8) Kasas, S.; Thomson, N. H.; Smith, B. L.; Hansma, H. G.; Zhu, X. S.; Guthold, M.; Bustamante, C.; Kool, E. T.; Kashlev, M.; Hansma, P. K. *Biochemistry* **1997**, *36*, 461–468.
(9) Ellis, D. J.; Dryden, D. T. F.; Berge, T.; Edwardson, J. M.; Henderson, R. M. *Nat. Struct. Biol.* **1999**, *6*, 15–17.
(10) Berge, T.; Ellis, D. J.; Dryden, D. T. F.; Edwardson, J. M.; Henderson, R. M. *Biophys. J.* **2000**, *79*, 479–484.
(11) van Noort, J.; van der Heijden, T.; Dutta, C. F.; Firman, K.; Dekker, C. *Nucleic Acids Res.* **2004**, *32*, 6540–6547.
(12) Fowler, J. D.; Suo, Z. *Chem. Rev.* **2006**, *106*, 2092–2110.
(13) Bollum, F. J. *Terminal Deoxynucleotidy Transferase*, 3rd ed.; Academic Press: New York, 1974; Vol. 10, pp 145–171.
(14) Hyone-Myong, E. *Enzymology Primer for Recombinant DNA Technology*, 2nd ed.; Academic Press: New York, 1996; Vol. 1, pp 477–489.
(15) Gubler, U.; Hoffman, B. J. *Gene* **1983**, *25*, 263–269.
(16) Maxam, A. M.; Gilbert, W. *Proc. Natl. Acad. Sci. U.S.A.* **1977**, *74*, 560–564.
(17) Chow, D. C.; Lee, W. K.; Zauscher, S.; Chilkoti, A. *J. Am. Chem. Soc.* **2005**, *127*, 14122–14123.
(18) Glass, R.; Moller, M.; Spatz, J. P. *Nanotechnology* **2003**, *14*, 1153–1160.
(19) Förster, S.; Abetz, V.; Müller, A. H. E. *Adv. Polym. Sci.* **2004**, *166*, 173–210.
(20) Allen, C.; Maysinger, D.; Eisenberg, A. *Colloids Surf., B* **1999**, *16*, 3–27.
(21) Alemdaroglu, F. E.; Herrmann, A. *Org. Biomol. Chem.* **2007**, *5*, 1311–1320.
(22) Alemdaroglu, F. E.; Ding, K.; Berger, R.; Herrmann, A. *Angew. Chem., Int. Ed.* **2006**, *45*, 4206–4210.
(23) Alemdaroglu, F. E.; Wang, J.; Börsch, M.; Berger, R.; Herrmann, A. *Angew. Chem., Int. Ed.* **2008**, *47*, 974–976.
(24) Ding, K.; Alemdaroglu, F. E.; Börsch, M.; Berger, R.; Herrmann, A. *Angew. Chem., Int. Ed.* **2007**, *46*, 1172–1175.
(25) Lee, W.-K.; Patra, M.; Linse, P.; Zauscher, S. *Small* **2007**, *3*, 63–66.
(26) Dormidontova, E. E. *Macromolecules* **1999**, *32*, 7630–7644.
(27) Nyrkova, I. A.; Semenov, A. N. *Macromol. Theory Simul.* **2005**, *14*, 569–585.
(28) Malmsten, M.; Lindman, B. *Macromolecules* **1992**, *25*, 5440–5445.
(29) Smith, S. B.; Cui, Y.; Bustamante, C. *Science* **1996**, *271*, 795–799.
(30) Rivetti, C.; Walker, C.; Bustamante, C. *J. Mol. Biol.* **1998**, *280*, 41–59.
(31) Tinland, B.; Pluen, A.; Sturm, J.; Weill, G. *Macromolecules* **1997**, *30*, 5763–5765.
(32) David, I. B. *An Introduction to Polymer Physics*, 1st ed.; Cambridge University Press: Cambridge, UK, 2002; pp 72–76.
(33) Murphy, M. C.; Rasnik, I.; Cheng, W.; Lohman, T. M.; Ha, T. J. *Biophys. J.* **2004**, *86*, 2530–2537.
(34) Olson, W. K. *Macromolecules* **1975**, *8*, 272–275.
(35) Mortensen, K. *J. Phys. (Paris)* **1996**, 103–124.

MA701937U